Applied Catalysis B: Environmental 182 (2016) 172–183

Contents lists available at ScienceDirect

Applied Catalysis B: Environmental

journal homepage: www.elsevier.com/locate/apcatb

The advanced removal of benzene from aerosols by photocatalytic oxidation and adsorption of Cu–TiO_2/PU under visible light irradiation

Thanh-Dong Pham, Byeong-Kyu Lee*, Chi-Hyeon Lee

Department of Civil and Environmental Engineering, University of Ulsan, Daehakro 93, Namgu, Ulsan 680-749, Republic of Korea

ARTICLE INFO

Article history:
Received 14 May 2015
Received in revised form 31 August 2015
Accepted 11 September 2015
Available online 12 September 2015

Keywords:
Cu doping
Air purification
Benzene removal
Mineralization
Humidity effects

ABSTRACT

In this study, we used $Cu(NO_3)_2$ as a precursor of Cu dopants, which defected the TiO_2 lattice and copper oxides, which in turn distributed on the TiO_2 surface to enhance the photocatalytic oxidation activity of the TiO_2. Porous polyurethane (PU) was used as a substrate for the immobilization of the enhanced TiO_2, to increase the adsorption capacity of the photocatalyst. Therefore, the synthesized Cu–TiO_2, immobilized on PU (Cu–TiO_2/PU) materials, exhibited both improved photocatalytic oxidation and adsorption activity for the effective removal of benzene from indoor aerosols. The benzene removal, by Cu–TiO_2/PU under visible light conditions, was due to the combination of improved adsorption and photocatalytic oxidation. The removal of benzene from the aerosol was strongly dependent on humid environmental conditions, and the amount of Cu in the Cu/TiO_2. Optimal humidity conditions and the amount of Cu in the Cu/TiO_2, for the photocatalytic oxidation of benzene in the aerosol by the Cu–TiO_2/PU photocatalyst, were 60% RH and 6 wt%, respectively. Under visible light irradiation, and at a relative humidity of 60% RH, the 6% Cu–TiO_2/PU material removed 86% of the benzene in 100 ppm inlet gas, while 91% of the removed amount was mineralized into CO_2 and H_2O.

1. Introduction

A lot of volatile organic compounds (VOCs), with boiling points from 50 to 250 °C, are emitted from various sources, such as: industrial processes, transport and house-hold activities [1]. In addition, a significant amount of VOCs could be emitted from indoor facilities and wall surfaces. Many VOCs have been reported to have significant adverse impacts to the environment and human health [2]. In particular, some aromatic and chloro chemicals, such as benzene, chloroform and chloroethylene, are regulated as carcinogenic [3]. For the treatment of carcinogenic VOCs emitted from indoor facilities or vehicles, various physical, chemical and biological techniques, including: adsorption, incineration, condensation, wet scrubbing, membrane separation, bioreaction and plasma oxidation, have been employed [4,5]. However, these technologies have still exhibited some disadvantages or limitations, in terms of broader application [6]. For example, the adsorption technology simply transfers organics from the gas phase to the solid phase, and subsequently requires further treatment processes, which means that this method would not be an economical option for the removal of large amounts of VOCs. The incineration and condensation technologies are cost-effective, as they are only used for the treatment of VOCs in moderate to high concentration. These techniques are limited, in terms of their practicality, as it pertains to controlling indoor carcinogens like benzene; this is because indoor emissions or concentrations are not typically high enough to make the application of these methods practical or economical.

Currently, the use of photocatalysts in photocatalytic oxidation, for the removal of VOCs, has been become a very attractive and promising alternative technology, particularly for indoor air purification [7,8]. It has already been reported that VOCs could be oxidized to carbon dioxide, water and simple mineral acids by TiO_2 photocatalysts, under or near UV irradiation [9]. TiO_2, a semiconductor, is usually used as an ideal photocatalyst since it is relatively cheap, non-toxic, highly stable from a chemical point of view and easily available [10,11]. However, one of the inherent disadvantages of the TiO_2 is that UV light (or near UV light) in the wavelength range ($\lambda < 400$ nm) must be used to initiate for the photocatalytic oxidation process. Thus the limitation of the applications of the photocatalysis, in the practical system, are associated with UV use and accompanied by safety issues and high energy consumption [12]. Therefore, numerous studies have been carried out to extend the absorption of the TiO_2 in the visible light range (400–700 nm) to overcome the disadvantages concerning the use of UV irradiation as an initiation source for photo-oxidation processes [10,12]. One of the most promising techniques for improving the visible light absorption of the TiO_2 photocatalyst is to use metals such as Cu, V, Cr, Mo, Fe, Co and W (as doping agents) to narrow the TiO_2

* Corresponding author. Fax: +82 52 259 2629.
E-mail address: bklee@ulsan.ac.kr (B.-K. Lee).

http://dx.doi.org/10.1016/j.apcatb.2015.09.023
0926-3373/

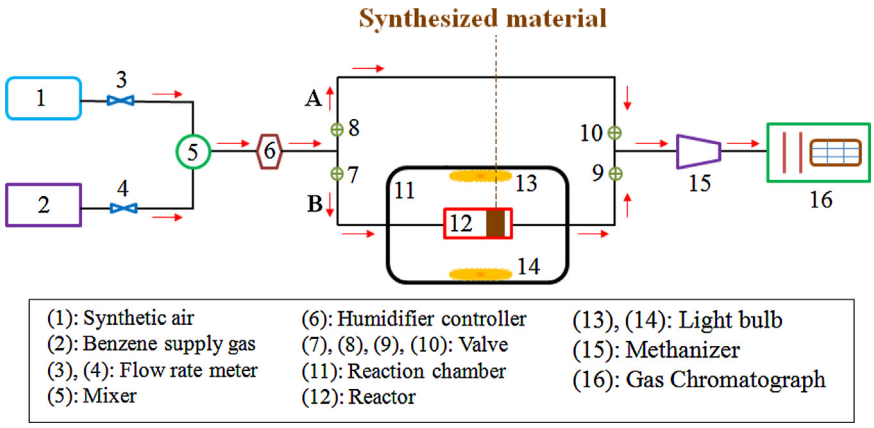

Fig. 1. The schematic diagram of the benzene removal system.

band gap (3.2 eV) [13,14]. This metal doping could also increase the electron–hole generation capacity of TiO_2, leading to enhancing the photocatalytic activity of the photocatalyst [14]. In our previous study, Cu was used as a doping agent to improve the photocatalytic disinfection activity of TiO_2, immobilized on glass fiber [15]. The synthesized Cu–TiO_2/GF exhibited high photocatalytic disinfection activity in the removal bioaerosol, even under visible light.

There are a few reports about the effects of Cu doped TiO_2 on the photocatalytic oxidation of VOCs in aerosols [16]. In our previous study, the synthesized Cu–TiO_2/GF could exhibit only photocatalytic activity; however, its adsorption ability seemed to be very low; this was because the Cu–TiO_2/GF used glass fiber, a material with a small specific surface area, which only acted as a substrate for the immobilization of the Cu doped TiO_2. Therefore, in this study, we used PU – a material with a high specific surface area – as a promising substrate to not only immobilize the Cu doped TiO_2, but also to increase the adsorption ability of the photocatalyst. Thus, the synthesized Cu doped TiO_2, immobilized on PU (Cu–TiO_2/PU), is expected to exhibit both improved adsorption and photocatalytic oxidation activity in the removal of the benzene (classified as class I carcinogenic VOCs by the International Agency for Research on Cancer) from aerosols, even under visible light irradiation [17]. In addition, the removal of the benzene from indoor aerosols is strongly affected by the concentration of water in the air stream [18–21]. The water could be adsorbed on the photocatalyst surface, hindering the further adsorption of the targeted contaminants [20]. The presence of water molecules is also considered to play an important role in the formation of the highly reactive hydroxyl radicals, directly affecting the photocatalytic oxidation process [22]. There are several discrepancies within the previous explanations, with regard to the moisture effect on the photocatalytic activity; therefore, in this study, we extended the previous theories, in an attempt to clarify the effects of humidity on the removal of benzene from indoor aerosols by adsorption and the photocatalytic oxidation of Cu–TiO_2/PU, under visible light conditions.

2. Materials and methods

2.1. Material synthesis

First, pristine PU was activated using a mixed solution of toluene, toluene-2,4-diisocyanate, and anhydrous triethylamine, to introduce isocyanate groups (NCO) onto its surface [23]. Second, titanium tetraisopropoxide (TTIP) was reacted with γ-aminopropyl triethoxysilane (APTES) to synthesize amino titanosiloxane, which contains Si—O—Ti bonds and an amine group (NH_2) [23]. Third, the activated PU was immersed into the amino titanosiloxane solution for 1 h, to fix the titanosiloxane on PU; this fixing occurred, based on the urea bond that forms as a result of the reaction between the isocyanate groups of the isocyanated PU, and the amino group (NH_2) of the amino titanosiloxane [23]. A 0.1 M $Cu(NO_3)_2$ solution, which was prepared by the dissolution of $Cu(NO_3)_2$ in deionized water at 60 °C, was slowly added (drop-wise) onto the amino titanosiloxane fixed on PU. The obtained material was cleaned using 1 M oxalic acid solution, then was irradiated with a UV light (60 W) for 5 h and then calcined under nitrogen at 200 °C for 5 h to produce Cu-doped TiO_2 fixed on PU (Cu–TiO_2/PU). The addition volume of $Cu(NO_3)_2$ solution was adjusted in order to synthesize 0, 2, 4, 6, 8 and 10% Cu–TiO_2/PU materials, which the ratios of Cu/TiO_2 had 0, 2, 4, 6, 8 and 10 wt%, respectively.

2.2. Material characterization

A Thermo Fisher K-Alpha X-ray Photoelectron Spectrometer system was used to obtain the X-ray photoelectron spectroscopy (XPS) spectra of the Cu–TiO_2/PU materials. The Gaussian multipeak shapes were applied to fit the Cu $2p_{3/2}$ and Ti $2p_{3/2}$ peaks in the obtained XPS spectra, to determine the elemental state of the copper and titanium in the synthesized materials. X-ray diffraction (XRD) measurements of Cu–TiO_2/PU were performed, using a Bruker AXN model with a Cu-Kα radiation (λ = 1.5418 Å) source, and operated at a scan rate of 0.02° s^{-1} over a 2θ range of 10–80°. A Hitachi S-4700 scanning electron microscope (SEM) was used to determine the surface morphology of the Cu–TiO_2/PU, with different ratios of Cu/TiO_2. Before the SEM analysis, all the samples were coated with Pt to increase the conductivity of the sample surface. The surface area (S_{BET}) of the synthesized Cu–TiO_2/PU materials were calculated, based on the Brunauer–Emmett–Teller (BET) isotherm carried out by nitrogen adsorption and desorption at 77 K. An Evolution 300 spectrophotometer (UV-1700 Shimadzu) was used to measure the light absorption spectra of the Cu–TiO_2/PU in the wavelength range 300–700 nm.

2.3. Experiments for the removal of benzene

A continuous online system for experiments involving the removal of benzene from aerosols, using Cu–TiO_2/PU materials was shown in Fig. 1. A cylinder containing 1000 ppm benzene in nitrogen gas was used as the benzene supply gas. The benzene gas was mixed with synthetic air, containing 20.5% vol O_2 and 79.5% vol N_2, to obtain a gas mixture of benzene concentration. Flow rate meters (3) and (4) were controlled to achieve a flow rate of 100 mL/min of 100 ppm benzene in the gas mixture. The humidity controller was employed to control the relative humidity of the gas mixture. Before the benzene removal experiments, valves (7) and (9) were closed, and valves (8) and (10) were opened to ori-

ent the input gas through direction A to a gas chromatograph (GC) system to re-check the concentration of the benzene in the gas mixture. When the benzene concentration in the 100 mL/min flow of mixed gas was stabilized at 100 ppm, valves (8) and (10) were closed and valves (7) and (9) were opened to orient the input gas toward direction B, where it passed through a reactor containing 36 cm^3 of the synthesized Cu–TiO_2/PU porous material. The reactor (2 cm × 4 cm × 15 cm) was placed in the center of a reaction chamber, which was a cask (25 cm × 50 cm × 50 cm) with a dark cover. Thus, the gaseous benzene was fed into the reactor with the hourly space velocity of 50 h^{-1} and the weight hourly space velocity of 0.0037 h^{-1}. The top and bottom of the reactor were made of quartz to allow easy passage of the visible light, generated from two 20 W light bulbs placed at the top and the bottom of the reaction chamber, through the reactor wall to excite electron generation for photocatalytic processes (Fig. 1).

Two light bulbs could generate visible light (400–700 nm) with a power density of 0.05 W/cm^2 in the reaction chamber. The benzene concentration in the effluent gas, passing through reactor, was analyzed using the gas chromatograph (GC) system, which included a GC (Varian CP-3800) equipped with a flame ionization detector (FID) and a packed column (Porapak Q 80/100 2 m × 2 mm). A methanizer, using Ni catalyst, was also integrated into the GC system for the analysis of the CO and CO_2 contents in the effluent gas. The effluent gas was sent to the GC system by an auto sampling injector, which could automatically inject 100 μL of the effluent gas into the packed column, in intervals of 10 min. Helium was used as a carrier gas, with a flow rate of 25 mL/min. The benzene removal experiments were carried out under both a darkened condition and visible light irradiation, achieved by turning the bulbs off/on, respectively. The reaction start time ($t_0 = 0$) was estimated to be the time when valves (7) and (9) were opened. The benzene removal efficiency and degree of mineralization, which is representative of the conversion degree of benzene into CO and CO_2, were evaluated using Eqs. (1) and (2), respectively:

$$\text{Benzene removal efficiency}(\%) = \frac{C_0 - C_t}{C_0} \times 100\% \quad (1)$$

$$\text{Mineralization degree} = \frac{C_{tCO_2}}{6 \times (C_0 - C_t)} \times 100\% \quad (2)$$

where: C_0 (100 ppm) is the concentration of benzene at the reaction start time ($t_0 = 0$), and C_t and C_{tCO2} are the concentrations of benzene and CO_2 at reaction time ($t_i = t$), respectively.

3. Results and discussion

3.1. Material properties

3.1.1. Surface elemental states

Fig. 2 shows the high-resolution XPS spectra for the Cu $2p_{3/2}$ peaks of copper in 2, 4, 6, 8 and 10% Cu–TiO_2/PU. The Cu $2p_{3/2}$ peaks of copper in Cu–TiO_2/PU consisted of two different peaks, observed at 932.18 and 933.48 eV, which were attributed to the binding energies of Cu $2p_{3/2}$ of the Cu^+ and Cu^{2+} states, respectively [24,25]. Most of the Cu^+ and Cu^{2+} existed in the forms of Cu_2O and CuO oxides, respectively. The CuO oxide could be produced from the decomposition of $Cu(NO_3)_2$ under the effect of the UV irradiation and calcination temperature, during the preparation processes [15,25,26]. The UV irradiation and oxalic acid, rolled as a cleaner for the cleaning process, could also reduce Cu^{2+} into Cu^+ during the decomposition of $Cu(NO_3)_2$, to form Cu_2O [26–29]. The obtained HRTEM results confirm the existences of CuO and Cu_2O blending with TiO_2 (Fig. 3). The lattice spacing is approximately 0.246 nm, which is close to the interlayer distance of the (1 1 1) crystal plane of the Cu_2O (Fig. B2) [30]. The lattice spacing of approximately 0.231 and 0.301 nm correspond to the interlayer distance of the (1 1 1) and (1 1 0) crystal planes of CuO [31,32]. As compared to XRD pattern of TiO_2/PU, the XRD pattern of Cu–TiO_2/PU shows additional occurrences of peaks at 27.5° and 36.1°, corresponding to rutile peaks of TiO_2 (Fig. 4). Rutile peaks occurred due to the Cu dopants, which defected the anatase phase, resulting in the faster formation and growth of rutile nuclei, as well as rutile crystals [33–35]. Moreover, the Cu doping led to oxygen vacancies, which could also accelerate the anatase-rutile phase transformation or the formation of the rutile phase in the TiO_2 [36,37]. The HRTEM also shows the formation of the rutile phase in the Cu–TiO_2/PU resulted from the incorporation of Cu into the TiO_2 lattice. The TiO_2 anatase peak, at 25.4° in the XRD pattern of Cu–TiO_2/PU, was more left-shifted and broadened than that of the TiO_2/PU. This observation also indicates that the Cu dopants incorporated into the TiO_2 lattice, leading to distortions in the crystal lattice. Cu dopants could defect and sub-

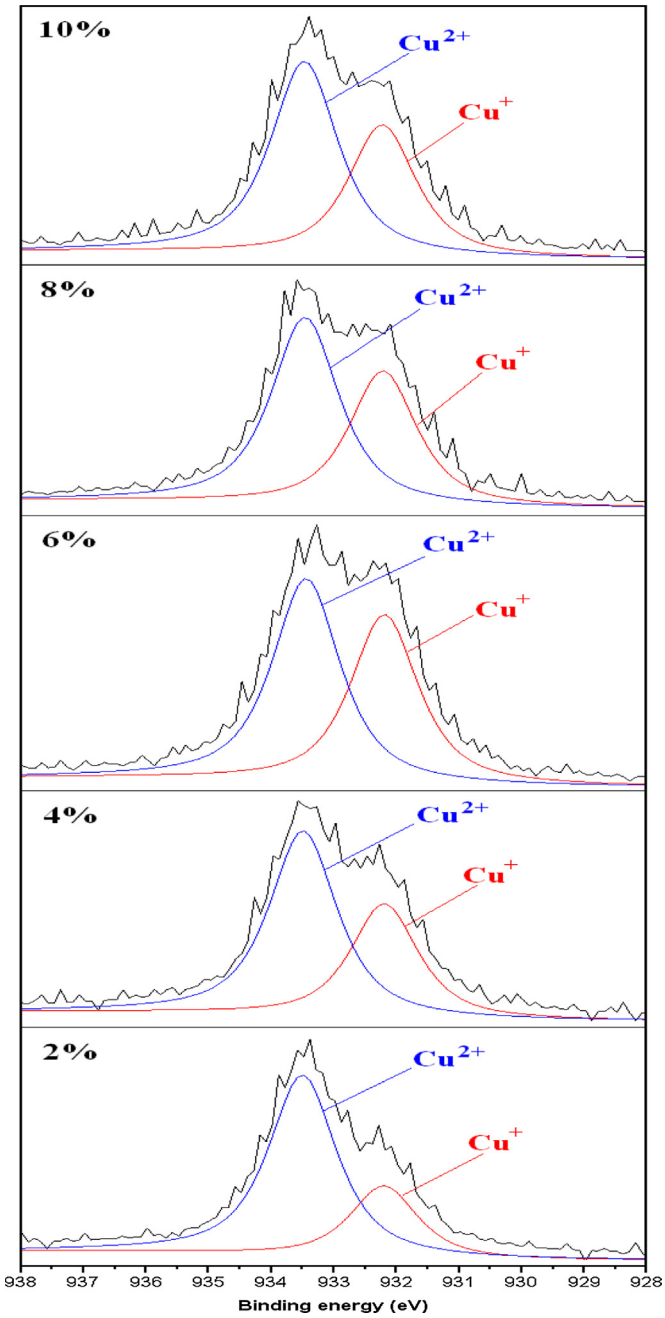

Fig. 2. High-resolution XPS spectra of Cu $2p_{3/2}$ in X% Cu–TiO_2/PU.

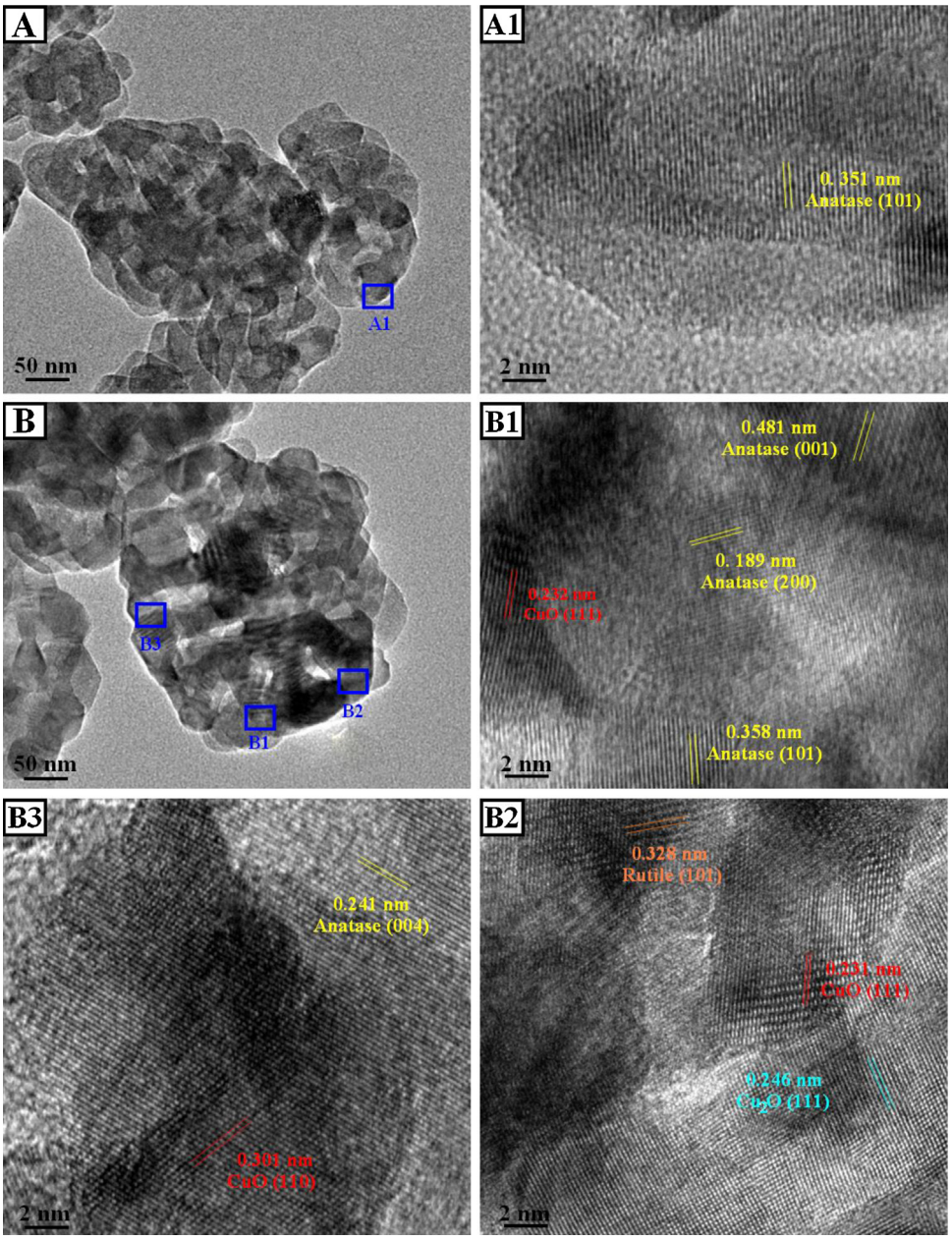

Fig. 3. TEM images of TiO_2/PU (A) and Cu–TiO_2/PU (B); HRTEM images of the selected areas in the TEM images of TiO_2/PU (A1) and Cu–TiO_2/PU (B1, B2 and B3).

stitute the Ti^{4+} ions in the TiO_2 lattice by forming Cu—O—Ti bonds [29,38]. Due to the incorporation of Cu into the TiO_2 lattice, the interlayer distance of the (1 0 1) crystal plane of the TiO_2 anatase also slightly increased (Fig. A1 and B1). Therefore, the elemental states of the copper in Cu–TiO_2/PU included copper oxides (Cu_2O and CuO), which are blended with the TiO_2, and the copper dopants existed in the TiO_2 lattice in the form of Cu—O—Ti bonds.

The Cu^+/Cu^{2+} ratios in the Cu–TiO_2/PU, which are proportional to the ratios of (the area under the Cu^+ peak)/(the area under the Cu^{2+} peak) in the XPS spectra, are shown in Table 1. The Cu^+/Cu^{2+} ratios rapidly increased with the increasing Cu/TiO_2 ratios, until the ratio of Cu/TiO_2 in Cu–TiO_2/PU reached 6 wt%. However, with the further increase of the Cu/TiO_2 ratios above 6% wt, the Cu^+/Cu^{2+} ratios slightly decreased. The reduction of Cu^{2+} into Cu^+, which resulted from the incorporation of Cu ions into the TiO_2 lattice as well as from the oxalic acid cleaning and UV irradiation processes (rolled as reducing agents) led to oxygen vacancies in the TiO_2 and CuO lattice [39,40]. The formation of oxygen vacancies led to a certain degree of limitation in the Cu^{2+} reduction [41]. Therefore, the Cu^+/Cu^{2+} ratios seem to decrease when the Cu/TiO_2 ratios are higher than 6 wt%. It was determined that the maximum ratios of Cu^+/Cu^{2+} in the Cu–TiO_2/PU were approximately 44.94%, when the Cu/TiO_2 ratio was 6 wt%.

The obtained XPS spectra indicate that the elemental state of titanium in the TiO_2/PU was only Ti^{4+}, while the elemental states of titanium in the synthesized Cu–TiO_2/PU materials were composed of both Ti^{4+} and Ti^{3+} (Fig. 5) [42,43]. The formation of Ti^{3+} in the Cu–TiO_2/PU could be due to the effect of the Cu dopant, which defected the TiO_2 lattice. The Cu doping led to the oxygen vacancies in the TiO_2 lattice, resulting in the reduction of Ti^{4+} into Ti^{3+} [44,45]. Ti^{3+} could more easily generate excited electrons than Ti^{4+} because the electron number of Ti^{3+} (19) is higher than that of Ti^{4+} (18), and thus the electrons in Ti^{4+} are more strongly bound to the titanium nuclei than those in Ti^{3+} [46]. Therefore, the Ti^{3+} is widely accepted to have greater photocatalytic activity than the Ti^{4+} [46]. It is also known that the photocatalytic activity of TiO_2 positively relates

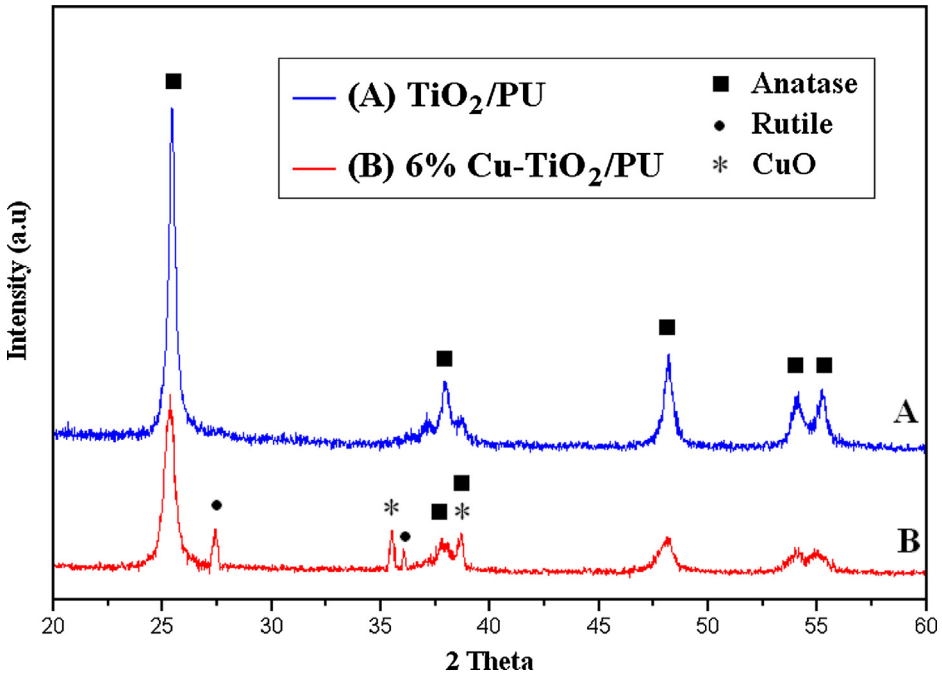

Fig. 4. XRD patterns of the TiO_2/PU and 6% Cu–TiO_2/PU.

Table 1
The ratios of Cu^+/Cu^{2+}, Ti^{3+}/Ti^{4+}, the BET surface area and the band gap energies of the Cu–TiO_2/PU materials.

	Cu^+/Cu^{2+} ratios (%)	Ti^{3+}/Ti^{4+} ratios (%)	BET surface area(m^2/g)	Band gap energy (eV)
TiO_2/PU	–	0	111.4	3.20
2% Cu–TiO_2/PU	28.91	16.7	137.5	3.05
4% Cu–TiO_2/PU	38.53	20.5	154.9	2.92
6% Cu–TiO_2/PU	44.94	25.4	166.3	2.85
8% Cu–TiO_2/PU	42.12	26.2	179.2	2.79
10% Cu–TiO_2/PU	40.7	26.4	159.1	2.75

with the concentration of Ti^{3+} in its lattice [46]. Table 1 also shows the calculated Ti^{3+}/Ti^{4+} ratios in the Cu–TiO_2/PU samples, which are proportional to the ratios of (the area under the Ti^{3+} peak)/(the area under the Ti^{4+} peak) in the XPS spectra. The obtained results illustrated that the trend of the Ti^{3+} contents in the Cu–TiO_2/PU increased rapidly with the increasing Cu/TiO_2 ratios, and gradually stabilized when the Cu/TiO_2 ratio rose above 6 wt%. The increasing in Ti^{3+} contents in Cu–TiO_2/PU could be due to the role of the Cu dopants defected into TiO_2 lattice, leading to oxygen vacancies or the reduction of Ti^{4+} into Ti^{3+}. However, the defect of copper into the TiO_2 lattice showed a certain limit; hereafter, further significant defects of copper into the TiO_2 lattice were not observed even with the further increase of the Cu/TiO_2 ratios.

3.1.2. Surface morphology and surface area

Fig. 6 shows the SEM and elemental mapping images of Cu and Ti in the selected areas of the synthesized TiO_2/PU, and the 2, 4, 6, 8 and 10% Cu–TiO_2/PU materials. The TiO_2 in the TiO_2/PU was smoothly immobilized on the PU surface as a thin layer (Fig. 6**A**). The elemental mapping images shows that the Cu_2O and CuO existed as micro particles on surface the TiO_2 layer. Because of the existence, the surface of Cu–TiO_2/PU materials was more roughness than the surface of the TiO_2/PU. The N_2 adsorption–desorption isotherms also indicated that the TiO_2/PU surface mostly contained narrow slit pores while the Cu–TiO_2/PU surface contained the ink-bottle-shaped pores and randomly folded sheets of solid (see the Supplementary material). The degree of surface roughness seemed to increase with the increasing Cu/TiO_2 ratios. The coverage of the micro particles of copper oxides on TiO_2 surface is also positively related with the Cu/TiO_2 ratios. When the Cu/TiO_2 ratios increased up to 10% wt, the copper oxides were clustered into larger particles covering the TiO_2 layer (Fig. 6**F**).

Table 1 shows that the BET surface area of the synthesized TiO_2/PU (110.4 m^2/g) was not only greatly higher than that of the PU (30.46 m^2/g) but also much higher than the surface area of commercial TiO_2 powder (60 m^2/g) [23,47]. This result indicates that the immobilization of TiO_2 onto surface of honeycomb-structure PU greatly increased the surface area of TiO_2. The immobilization could minimize the coagulation of the TiO_2 particles leading to increase its surface area. The obtained BET results also indicate that the surface areas of the Cu–TiO_2/PU materials were much higher than that of TiO_2/PU (Table 1). This could be due to role of the copper oxides, which increased the degree of surface roughness as described above, leading to an increase in the surface areas. The increase in surface area could lead to increase in adsorption ability of the synthesized materials. The BET surface areas of the Cu–TiO_2/PU samples also greatly increased with the increasing Cu/TiO_2 ratios, up to 8 wt%, whereafter a slight decrease was observed for 10 wt%. This could be due to the greater gathering or clustering of the copper oxides onto the larger particles at the high ratios of Cu/TiO_2 (such as 10 wt%) (Fig. 6**F**).

3.1.3. Optical properties

Fig. 7 shows the UV–vis optical absorption spectra of the TiO_2/PU and 2, 4, 6, 8 and 10% Cu–TiO_2/PU materials. The spectra indicate that the TiO_2/PU inherited the TiO_2 optical absorption properties, which displays absorption only in the UV light region, with the

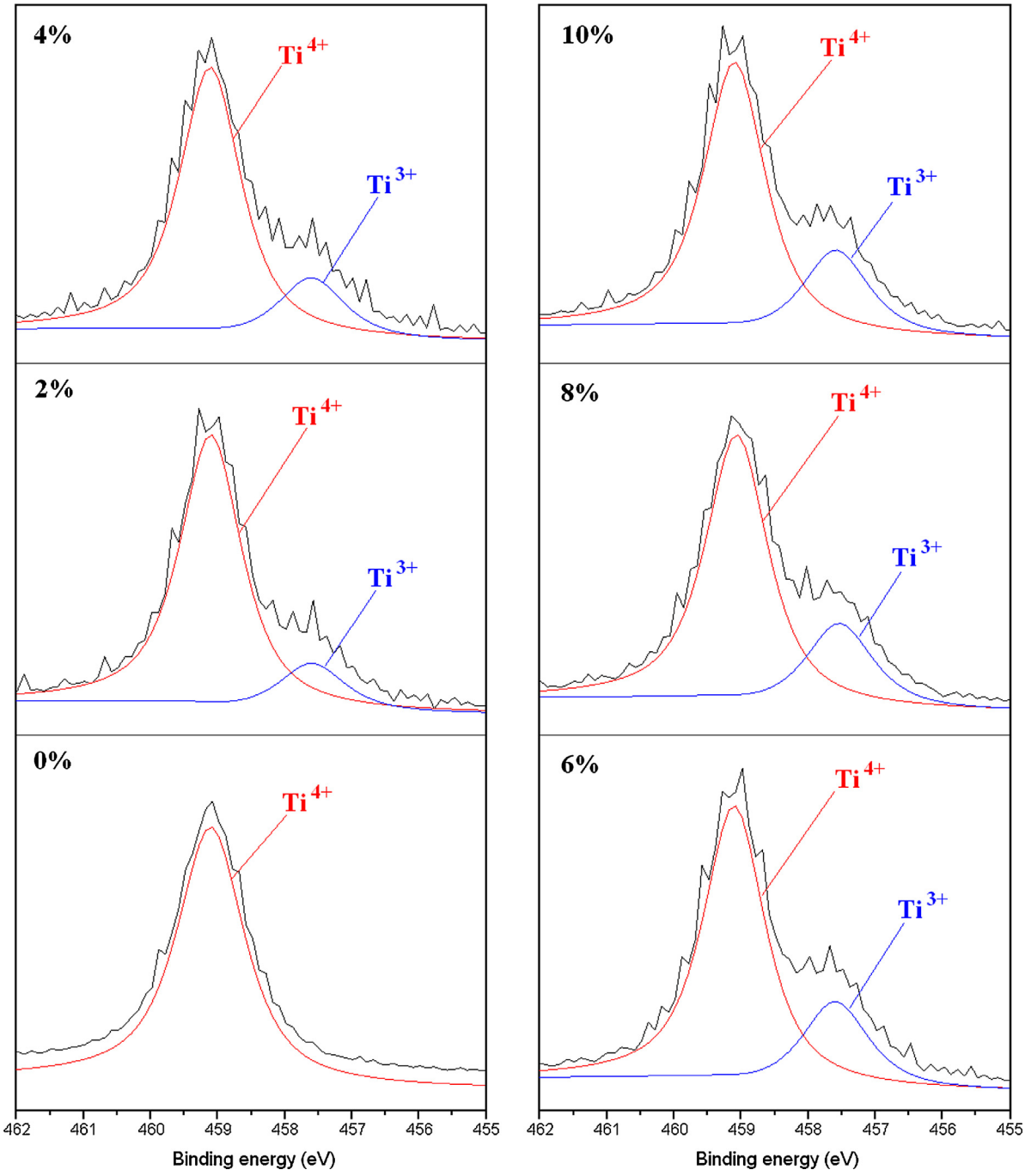

Fig. 5. High-resolution XPS spectra of Ti $2p_{3/2}$ in *X*% Cu–TiO_2/PU.

absorption edge around 370 nm [48,49]. The Cu–TiO_2/PU materials exhibited a more significant enhancement of light absorption in the visible region than the TiO_2/PU did. The UV–vis adsorption spectra show that the light absorption ability of the Cu–TiO_2/PU increased with the increasing weight fraction of the Cu in Cu/TiO_2 up to 6 wt% (Fig. 7). The light absorption enhancement of Cu–TiO_2/PU could be due to the role of the Cu dopants, which defected the TiO_2 lattice, leading to oxygen vacancies and the formation of Ti^{3+} in the TiO_2 lattice. The oxygen vacancies could minimize the energy level of the conduction band of the TiO_2, leading to increasing the light absorption ability of the doped TiO_2 materials [50]. The occurrence of Ti^{3+} and copper dopants in the doped TiO_2 lattice (proved in Section 3.2.1) could also create an intermediate band between the valance band and the conduction band of TiO_2, leading to enhancing the electron–hole pair separation efficiency of TiO_2 and the light absorption enhancement of the Cu–TiO_2/PU [50]. In addition, the copper oxides (CuO and Cu_2O) that formed on the surface of the TiO_2 layer could combine with TiO_2 to create a suitable semiconductor–semiconductor system. In the system, copper oxides could act as an electron carrier, to transfer electrons generated from the valence band to the conduction band of TiO_2 or an accepter [51]. Copper oxides could also act as an electron sink, to trap the separated electrons and prevent the recombination of electrons and holes, leading to increasing the electron–hole pair separation efficiency of TiO_2 [15]. Therefore, the combination between cooper oxides and the TiO_2 contributed to the enhancement of the light absorption of the synthesized material. When the Cu/TiO_2 ratios increased to high values (such as 8 and 10% wt) the

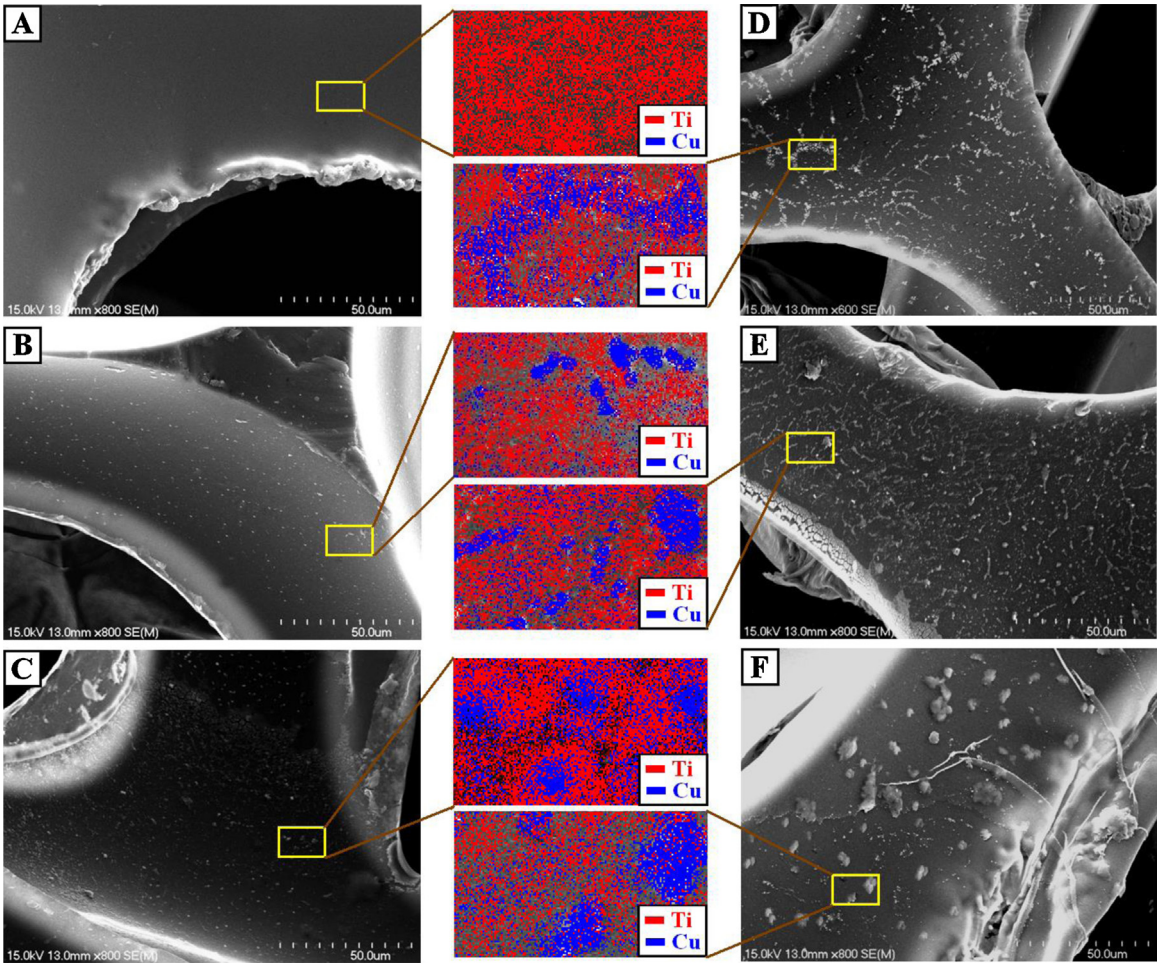

Fig. 6. SEM and elemental mapping images of Cu and Ti in the selected areas of TiO_2/PU (A), and 2% (B), 4% (C), 6% (D), 8% (E) and 10% (F) Cu–TiO_2/PU.

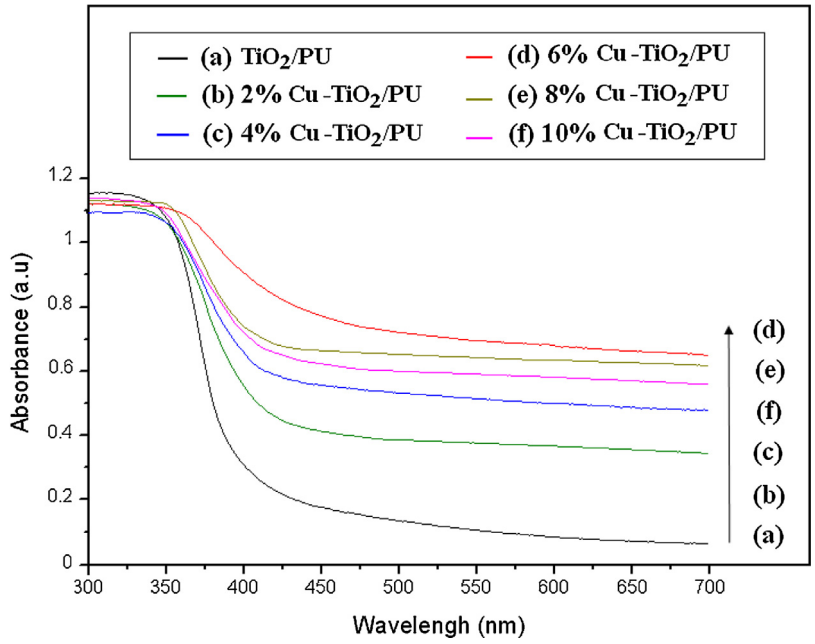

Fig. 7. UV–vis absorption spectra of TiO_2/PU, and 2, 4, 6, 8 and 10% Cu–TiO_2/PU.

light absorption of the Cu–TiO_2/PU was slightly decreased (Fig. 7); this is because the copper oxides gathered into larger particles on the surface of the TiO_2. The large particles eclipsed the light reaching to the TiO_2 surface, resulting in a decrease in light absorption [52]. In addition, the gathering of copper oxide particles led to an uneven distribution of the particles on the TiO_2 layer or a

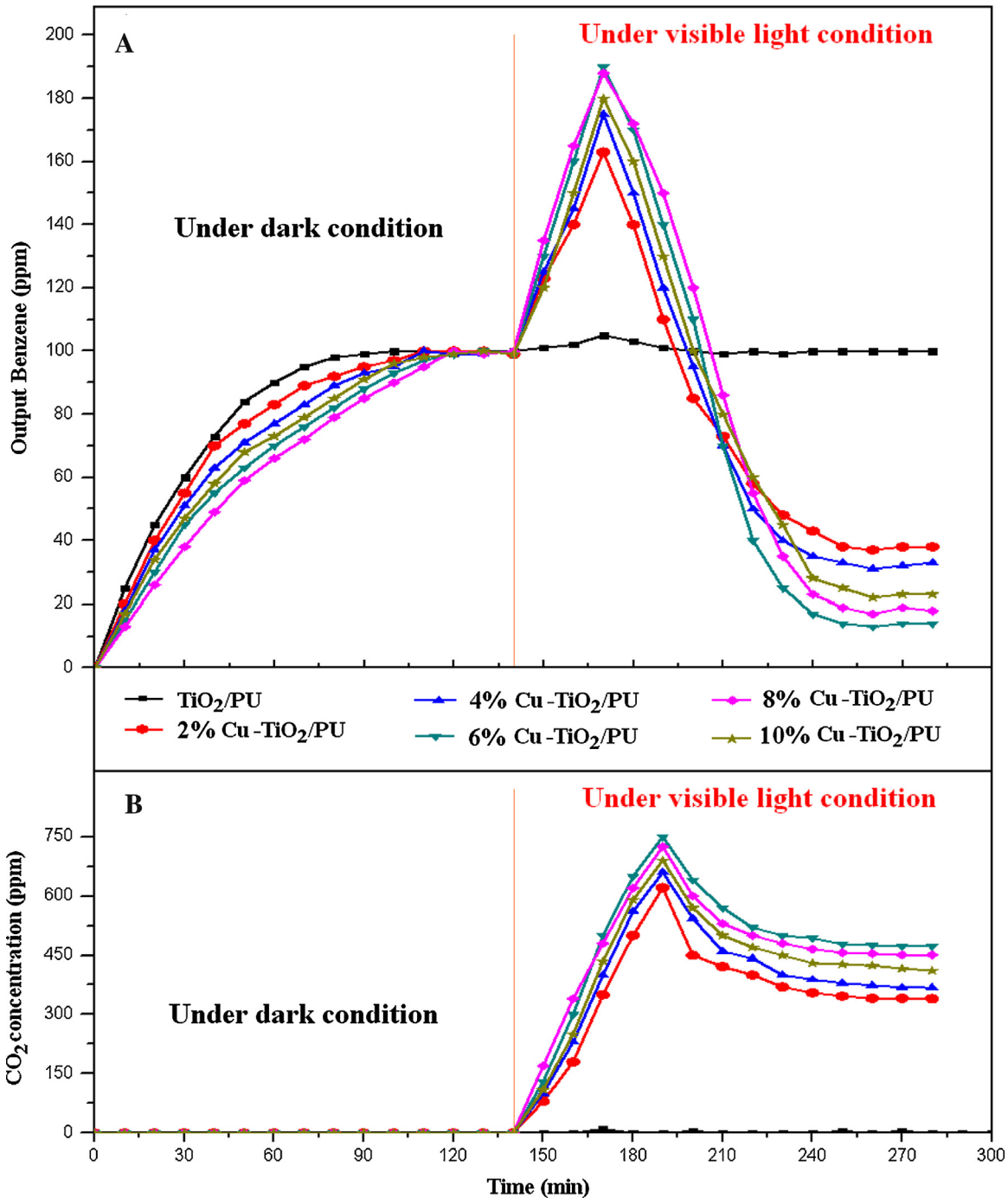

Fig. 8. Benzene removal (A) and generated CO_2 concentration (B) by *X*% Cu–TiO_2/PU under dark and then visible light conditions.

decrease in the interfacial surface between the copper oxides and the TiO_2. Therefore, the copper oxides could not act as an effective electron carrier/sink to enhance the electron–hole pair separation efficiency of the TiO_2 and, consequently, decreased the light absorption efficiency of the Cu–TiO_2/PU at high ratios of Cu/TiO_2 (8 and 10 wt%).

A Tauc plot, combined with the Kubelka-Munk method, was used to estimate the band gap energies of the synthesized Cu–TiO_2/PU, as shown Table 1 and Fig. S4 (see the Supplementary materials) [53,54]. The obtained results show that the band gap energy of Cu–TiO_2/PU was gradually decreased with increase in the Cu/TiO_2 ratios. This also due to Cu dopants defecting into the TiO_2 lattice to form Ti^{3+}, which could create an intermediate band between the valance band and the conduction band of TiO_2 led to decrease in band gap energy of the Cu–TiO_2/PU materials. It was also because CuO and Cu_2O existing on the surface of the TiO_2 layer could act as an electron carrier to transfer electrons generated from the valence band to the conduction band of TiO_2 thereby, decrease the band gap energy of TiO_2 [51]. On other hand, when the Cu/TiO_2 ratios increased the surface of the Cu–TiO_2/PU materials were more covered by the copper oxide. When the proportion of copper oxides covering the surface of the Cu–TiO_2/PU increased, the Cu–TiO_2/PU materials tended to closely exhibit the band gap energy of CuO and Cu_2O, which are approximately 1.2 and 2.1 eV, respectively, rather than the band gap energy of TiO_2 (3.2 eV) [55–57]. Therefore, the band gap energy

Table 2
The benzene removal efficiency and the mineralization degree, using Cu–TiO_2/PU, with different Cu/TiO_2 ratios under visible light conditions.

	Visible light condition A		Visible light condition B	
	Removal efficiency (%)	Mineralization degree (%)	Removal efficiency (%)	Mineralization degree (%)
2% Cu–TiO_2/PU	62.6	78.2	62.4	78.5
4% Cu–TiO_2/PU	67.5	83.1	67.7	83.9
6% Cu–TiO_2/PU	86.3	91.5	86.2	91.8
8%Cu–TiO_2/PU	82.1	87.4	82.4	82.1
10% Cu–TiO_2/PU	77.9	85.3	77.8	78.4

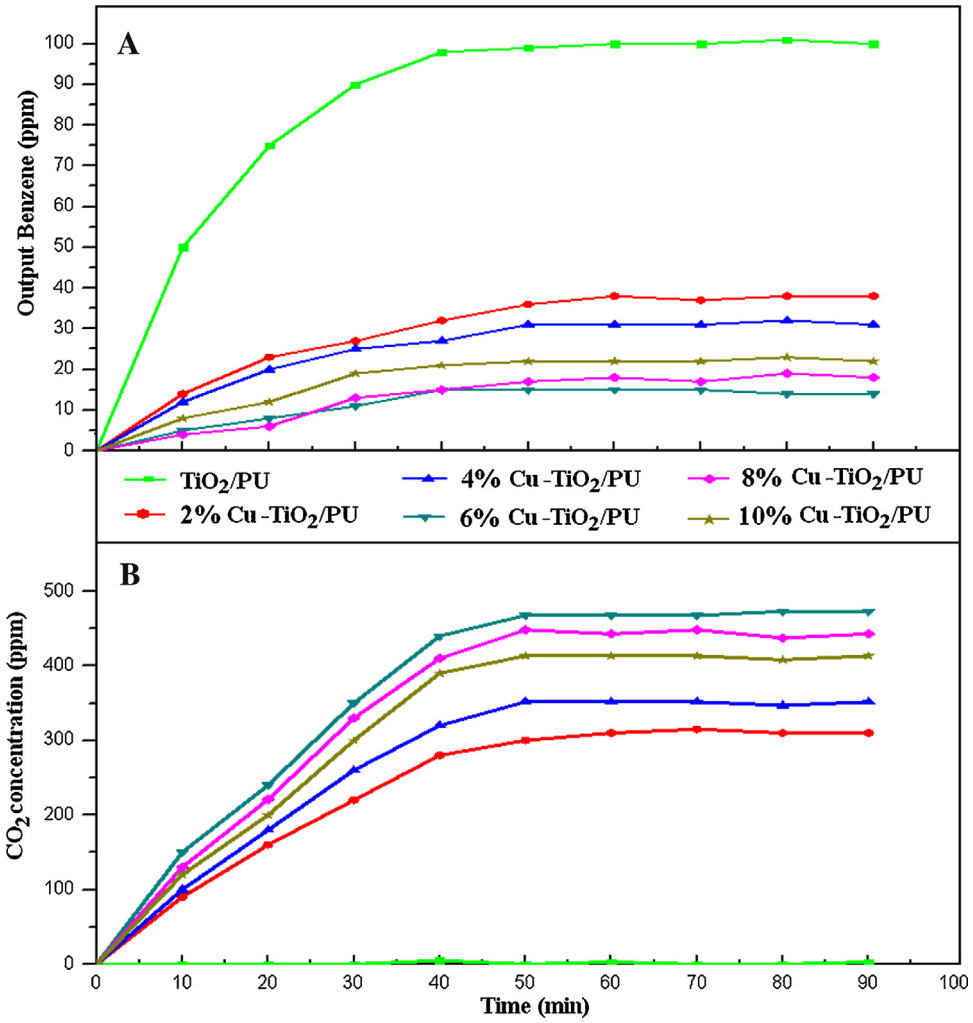

Fig. 9. Benzene removal (A) and generated CO_2 concentration (B) by *X*% Cu–TiO_2/PU under visible light conditions.

of the Cu–TiO_2/PU at high ratios of Cu/TiO_2 still tended to decrease, approaching those of copper oxides.

3.2. Benzene removal

3.2.1. Removal mechanism

The benzene removal experiments, using the TiO_2/PU, and 2, 4, 6, 8 and 10% Cu–TiO_2/PU, were conducted in darkened conditions for the first 140 min, after which visible light was provided for an additional 140 min (Fig. 8). Under the darkened conditions, the outlet benzene concentration gradually increased up to 100 ppm, which is the same as the inlet concentration and means that saturation occurred at 120 min (Fig. 8**A**). In addition, no CO_2 corresponding to the photocatalytic oxidation of benzene was detected (Fig. 8**B**); this indicates that, in darkened conditions, the benzene was removed by the Cu–TiO_2/PU only via adsorption. Before reaching to the saturation concentration (100 ppm), the slope of the outlet benzene concentration curves was inversely proportionate to the surface area of the Cu–TiO_2/PU materials, as shown in Table 1. It is known that a material that easily reaches adsorption saturation or has a low adsorption capacity, could exhibit a steep slope in its adsorption curve. A less steep slope indicates that the material could exhibit high adsorption capacity. Therefore, the benzene adsorption capacity of the Cu–TiO_2/PU materials was proportionate to their surface area. The benzene could be trapped on the surface of the Cu–TiO_2/PU by physical bond or electrostatic interaction between the aromatic ring of benzene and the cations on the surface of the Cu–TiO_2/PU [58].

When visible light was provided after saturation, the concentration of benzene passing through the TiO_2/PU material seemed

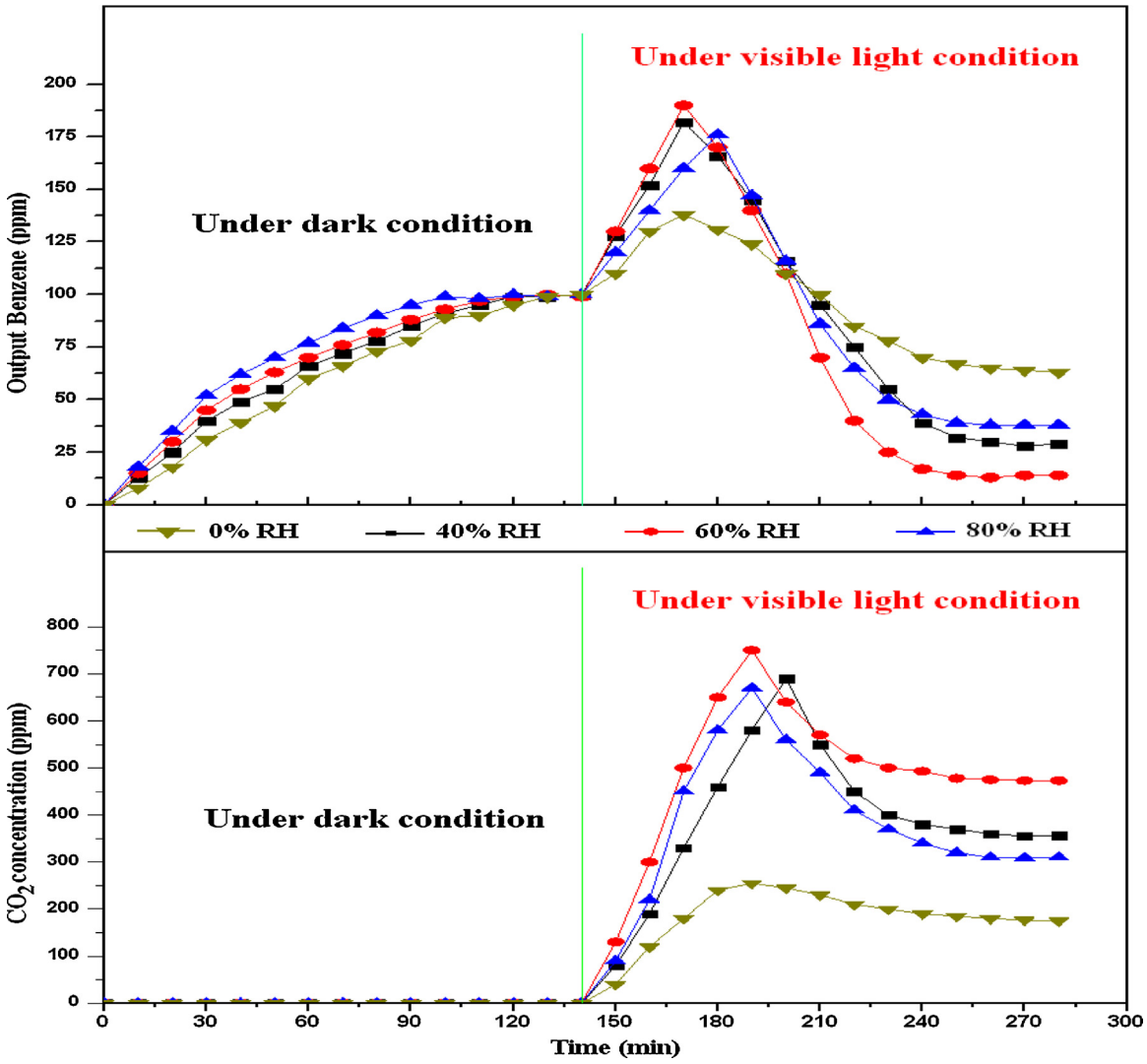

Fig. 10. Benzene removal (A) and generated CO_2 concentration (B) by 6% Cu–TiO_2/PU under relative humidity of 40, 60 and 80%.

to be unchanged; this indicates that the TiO_2/PU did not exhibit a significant photocatalytic oxidation activity to remove benzene under visible light conditions. However, the concentration of benzene passing through the Cu–TiO_2/PU materials displayed a sudden increase, exceeding the inlet concentration; the increase was due to desorption of the benzene adsorbed on the Cu–TiO_2/PU (rolled as an adsorbent) by the scrubbing of CO_2 generated from the photocatalytic oxidation of benzene by the Cu–TiO_2/PU (mainly acting as a photocatalyst) under visible light conditions. Because the Cu doping enhanced the electron–hole pair generation capacity and the separation efficiency of the TiO_2, the Cu–TiO_2/PU could generate electron-hole pairs even under visible light. In addition, these CuO and Cu_2O, existing on surface of TiO_2, are also semiconductors materials with the band gap energies of 1.2 and 2.1 eV, respectively [57]. Therefore, they could generate a certain number of electron–hole pairs under visible light. The generated electrons and holes then participated in reactions with the O_2 and/or the H_2O molecules in aerosol to produce oxy radicals, including hydroxyl radicals and superoxide radicals, which are strong oxidative agents. These radicals could then participate in the oxidation of benzene, causing it to decompose into CO_2 and H_2O, accompanied with a sharp increase in the CO_2 concentration, as shown in Fig. 8**B** [58,59]. The evaporation of the CO_2 generated from the photocatalytic oxidation of benzene could scrub certain amount of the benzene, which had initially been physical adsorbed on the Cu–TiO_2/PU surface during the darkened period, leading to desorption of benzene. Because of this desorption, the benzene concentration in the reactor suddenly increased. After the adsorbed benzene was almost completely desorbed, the outlet benzene concentration displayed a sharp decrease due to the continuous photocatalytic oxidation of benzene by the photocatalysts, accompanied by a decrease in the CO_2 concentration (Fig. 8B). The outlet benzene concentration reached steady values, ranging from around 10 to 30 ppm depending upon Cu content in Cu–TiO_2 (Fig. 8**A**).

When visible light was provided from the beginning of the benzene removal experiments ($t_0 = 0$), without an adsorption period under dark conditions, the outlet benzene concentrations passing through the Cu–TiO_2/PU materials reached stable values after 50 or 60 min (Fig. 9**A**). During the initial experimental period, the benzene was removed by both adsorption and the photocatalytic oxidation of benzene by the Cu–TiO_2/PU. However, the CO_2 gas, generated as a main product of the photocatalytic oxidation of benzene, disturbed the adsorption of benzene early on. Therefore, if the visible light was provided for longer than 50–60 min, the input benzene could only be removed by the photocatalytic oxidation activity of the Cu–TiO_2/PU.

3.2.2. Optimal Cu doping content

In the analysis of the slopes in the outlet benzene concentrations, expressed as a function of the reaction time when passed through the Cu–TiO2/PU under dark condition, the 8% Cu–TiO_2/PU exhibited the least steep slope (Fig. 8**A**). As discussed in the above section, the least steep slope corresponded to a high adsorption capacity. Therefore, among the Cu–TiO_2/PU materials, the 8% Cu–TiO_2/PU exhibited the highest adsorption capacity for benzene removal. This is because the 8% Cu–TiO_2/PU had the highest surface area among the synthesized Cu–TiO_2/PU materials; this fact confirms that the surface area values of the Cu–TiO_2/PU greatly affected the adsorption removal of benzene under the darkened conditions.

During visible light irradiation, the outlet benzene and CO_2 concentrations that passed through the Cu–TiO_2/PU materials under visible light conditions showed stable values (Figs. 8 and 9). Table 2 shows the calculated benzene removal efficiency and the mineralization degree of benzene into the CO_2 and H_2O by the Cu–TiO_2/PU, with different Cu/TiO_2 ratios. In particular, Table 2 compares the benzene removal and mineralization results from the visible light condition "A", which was provided after the benzene was adsorbed during the darkened period (0–140 min), and from the visible light condition "B", which was provided from the beginning of the benzene removal ($t = t_o$).

Both the benzene removal efficiency and the degree of mineralization by the Cu–TiO_2/PU, which showed similar results for both conditions "A" and "B", increased with the increase in the Cu/TiO_2 ratios (up to 6 wt%), and then gradually decreased with the further increase in the Cu/TiO_2 ratios (8 and 10 wt%). This was because the increase in the Cu/TiO_2 ratios led to an increase in the fraction of Cu dopants, which defected the TiO_2 lattice, and the copper oxides, which were distributed on the surface of the TiO_2. The content increase in the Cu dopants and copper oxides also increased the electron–hole pair generation capacity, the electron–hole separation efficiency and the lifespan of the excited electrons in the TiO_2, overall contributing to the increased photocatalytic oxidation of the benzene. However, the Cu dopants only defected the TiO_2 lattice to a certain limited level, as confirmed by the XPS analysis. The Cu doping effects seemed to reach this limit when the Cu/TiO_2 ratio was 6 wt%. In addition, the copper oxides tended to gather into larger particles at the high ratios of Cu/TiO_2 (8 and 10 wt%), resulting in decreasing photocatalytic oxidation activity and benzene removal efficiency (Table 2). The adsorption activity of the benzene could easily reach the saturation state, while the photocatalytic oxidation could be continuously maintained in a longer period of up to 5 h. The highest removal efficiency (86%) and degree of mineralization (92%) of the benzene were obtained from using 6 wt% Cu–TiO_2/PU as a photocatalyst, which would be an optimal dopant value, under visible light irradiation.

3.2.3. Effects of humidity

The benzene removal experiments, using 6% Cu–TiO_2/PU were carried out under darkened conditions for the first 140 min, and then under visible light irradiation for an additional 140 min as a function of the different relative humidity (RH) levels [0% (extreme dry), 40% (dry), 60% (moderate) and 80% (humid)] (Fig. 10). The obtained results indicate that the removal of benzene from aerosols, using Cu–TiO_2/PU was strongly affected by the humidity. Under the darkened condition, the extreme dry condition was found to be the best condition for the adsorption of the benzene, followed by the dry, the moderate and then humid conditions. This result indicates that the benzene adsorption capacity, using Cu–TiO_2/PU, was inversely proportional to the humidity level; this is because the increase in the humidity level or moisture content in the input gas stream increased the adsorption of the water molecules onto the Cu–TiO_2/PU surface, which has hydrophilic copper oxides [60,61]. The adsorption led to decrease in available sites on the surface of the Cu–TiO_2/PU for benzene adsorption resulting in the decreasing adsorption capacity of the benzene under moisture conditions, as compared to that under the dry condition.

Under the visible light, the best humidity condition for the photocatalytic oxidation of benzene was the moderate humidity level, followed by the dry, the humid conditions and extreme dry. Because the H_2O could react with generated holes on the surface of the Cu–TiO_2/PU to produce hydroxyl radicals, which are the main oxidative agents in the photocatalysis, the presence of proper water molecules is considered to play an important role in the photocatalytic oxidation processes [61,62]. Thus, the relative shortage of available H_2O molecules to generate hydroxyl radicals was the main reason for the lower photocatalytic oxidation of the benzene by the Cu–TiO_2/PU under extreme dry and dry conditions, as compared to that under intermediate conditions, which showed the best photocatalytic oxidation. Under extreme dry condition, the generated electrons and holes only reacted with the O_2 in aerosol to produce superoxide radicals leading to very low photocatalytic activity of the photocatalysis system. Ku et al. reported that- at too high humidity conditions-, water molecules occupied most of the most active sites on the photocatalyst surface while the photocatalytic oxidation of a gas occurred at the interface layer between the photocatalyst surface and the gas [62]. Therefore, at a high humidity level, the water hindered the photocatalytic oxidation process.

4. Conclusion

The synthesized Cu–TiO_2/PU adsorbed to remove the benzene from the aerosol under darkened conditions, and photocatalytically oxidized benzene into CO_2 and H_2O under visible light conditions. Both the adsorption and photocatalytic oxidation activity for the removal of benzene from the aerosol, using Cu–TiO_2/PU, were found to strongly depend on the humidity and the content of Cu in the Cu/TiO_2. The optimal humidity conditions for the adsorption and the photocatalytic oxidation of benzene by the Cu–TiO_2/PU was 40 and 60% RH, respectively. The optimal Cu content in Cu/TiO_2 for the photocatalytic oxidation and adsorption of benzene in aerosol were 6 and 8 wt%, respectively. The adsorption activity of a material could easily reach the saturation state, but photocatalytic oxidation could be continuously maintained for a long period, with visible light irradiation. Therefore, the photocatalytic oxidation was considered as a main factor for the removal of the benzene from the aerosol, using Cu–TiO_2/PU. Under visible light irradiation, and at an intermediate humidity of 60% RH, the 6% Cu–TiO_2/PU successfully removed 86% of the benzene in the 100 ppm inlet gas and 91% of the removed benzene was mineralized into CO_2 and H_2O.

Acknowledgments

This work was supported by a grant from the National Research Foundation of Korea (NRF), funded by the Ministry of Science, ICT and Future Planning (2013R1A2A2A03013138).

Appendix A. Supplementary data

Supplementary data associated with this article can be found, in the online version, at http://dx.doi.org/10.1016/j.apcatb.2015.09.023.

References

[1] M. Piumetti, D. Fino, N. Russo, Appl. Catal. B: Environ. 163 (2015) 277–287.
[2] K. Matsumoto, K. Matsumoto, R. Mizuno, M. Igawa, Atmos. Res. 97 (2010) 124–128.
[3] P.K.K. Louie, J.W.K. Ho, R.C.W. Tsang, D.R. Blake, A.H.K. Lau, J.Z. Yu, J. Yuan, X. Wang, M. Shao, L. Zhong, Atmos. Environ. 76 (2013) 125–135.
[4] Y. Li, Z. Fan, J. Shi, Z. Liu, W. Shangguan, Chem. Eng. J. 241 (2014) 251–258.

[5] A.M. Vandenbroucke, R. Morent, N.D. Geyter, C. Leys, J. Hazard. Mater. 195 (2011) 30–54.
[6] R.R. Gil, B. Ruiz, M.S. Lozano, M.J. Martín, E. Fuente, Chem. Eng. J. 245 (2014) 80–88.
[7] L. Zou, Y. Luo, M. Hooper, E. Hu, Chem. Eng. Process. 45 (2006) 959–964.
[8] W.K. Jo, K.H. Park, Chemosphere 57 (2004) 555–565.
[9] M. Hussain, N. Russo, G. Saracco, Chem. Eng. J. 166 (2011) 138–149.
[10] Y.H. Lin, T.K. Tseng, H. Chu, Appl. Cata. A: Gen. 469 (2014) 221–228.
[11] Y.T. Lin, C.H. Weng, F.Y. Chen, Chem. Eng. J. 248 (2014) 175–183.
[12] Z. Han, V.W. Chang, X. Wang, T.T. Lim, L. Hildemann, Chem. Eng. J. 218 (2013) 9–18.
[13] M. Nishikawa, R. Takanami, F. Nakagoshi, H. Suizu, H. Nagai, Y. Nosaka, Appl. Catal. B: Environ. 160–161 (2014) 722–729.
[14] E. Padmini, L.R. Miranda, Chem. Eng. J. 232 (2013) 249–258.
[15] T.D. Pham, B.K. Lee, Appl. Surf. Sci. 296 (2014) 15–23.
[16] Y. Lu, J. Liu, B. Lu, A. Jiang, C. Wan, J. Hazard. Mater. 182 (2010) 204–209.
[17] C. Treesubsuntorn, P. Thiravetyan, Atmos. Environ. 57 (2013) 317–321.
[18] J.F. Wu, C.H. Hung, C.S. Yuan, J. Photochem. Photobiol. A: Chem. 170 (2005) 299–306.
[19] X. Fu, L.A. Clark, W.A. Zeltner, M.A. Anderson, J. Photochem. Photobiol. A: Chem. 97 (1996) 181–186.
[20] K. Demeestere, J. Dewulf, B. De Witte, H. Van Langenhove, Appl. Catal. B: Environ. 60 (2005) 93–106.
[21] C. Raillard, V. Héquet, P.L. Cloirec, J. Legrand, Appl. Catal. B: Environ. 59 (2005) 213–220.
[22] U.F. Guo, D.Q. Ye, K.F. Chen, Y.-f Tian, Plasma Chem. Plasma Process. 26 (2006) 237–249.
[23] T.D. Pham, B.K. Lee, Chem. Eng. J. 275 (2015) 357–365.
[24] L.F. Chiang, R. Doong, J. Hazard. Mater. 277 (2014) 84–92.
[25] Y. Zou, S.Z. Kang, X. Li, L. Qin, J. Mu, Int. J. Hydrogen Energy 39 (2014) 15403–15410.
[26] E. Morrison, D. Gutiérrez-Tauste, C. Domingo, E. Vigil, J.A. Ayllón, Thin Solid Films 517 (2009) 5621–5624.
[27] Z. Zhang, J.B. Yi, J. Ding, L.M. Wang, H.L. Seng, S.J. Wang, J.G. Tao, G.P. Li, G.Z. Xing, T.C. Sum, C.H.A. Huan, T. Wu, J. Phys. Chem. C 112 (2008) 9579–9585.
[28] Q.D. Truong, M. Kakihana, J. Cryst. Growth 348 (2012) 65–70.
[29] A. Kubacka, M.J. Munoz-Batista, M. Fernández-García, S. Obregón, G. Colón, Appl. Catal. B: Environ. 163 (2015) 214–222.
[30] H. Xu, S. Ouyang, L. Liu, D. Wang, T. Kako, J. Ye, Nanotechnology 25 (2014) 165402–165410.
[31] X. Zou, H. Fan, Y. Tian, S. Yan, CrystEngComm 16 (2014) 1149–1156.
[32] E. Guo, L. Yin, Phys. Chem. Chem. Phys 17 (2015) 563–574.
[33] H.H.C.C.Y. Tsai, T.H. Kuo, Y.M. Chang, J.H. Liou, Aerosol Air Qual. Res. 13 (2013) 639–648.
[34] J. Nair, P. Nair, F. Mizukami, Y. Oosawa, T. Okubo, Mater. Res. Bull. 34 (1999) 1275–1290.
[35] H.W. Slamet, N.E. Purnama, S. Kosela, J. Gunlazuardi, Catal. Commun. 6 (2005) 313–319.
[36] M.S.P. Francisco, V.R. Mastelaro, Chem. Mater. 14 (2002) 2514–2518.
[37] S.B. Yuan, P. Meriaudeau, V. Perrichon, Appl. Catal. B: Environ. 3 (1994) 319–333.
[38] C.J. Lin, W.T. Yang, Chem. Eng. J. 237 (2014) 131–137.
[39] D.A. Firmansyah, T. Kim, S. Kim, K. Sullivan, M.R. Zachariah, D. Lee, Langmuir 25 (2009) 7063–7071.
[40] K. Lalitha, G. Sadanandam, V.D. Kumari, M. Subrahmanyam, B. Sreedhar, N.Y. Hebalkar, J. Phys. Chem. C 114 (2010) 22181–22189.
[41] J.Y. Kim, J.A. Rodriguez, J.C. Hanson, A.I. Frenkel, P.L. Lee, J. Am. Chem. Soc. 125 (2003) 10684–10692.
[42] H.W.P. Carvalhoa, A.P.L. Batistab, P. Hammer, T.C. Ramalho, J. Hazard. Mater. 184 (2010) 273–280.
[43] C.S. Kim, J.W. Shin, Y.H. Cho, H.D. Jang, H.S. Byun, T.O. Kim, Appl. Catal. A: Gen. 455 (2013) 211–218.
[44] R. Jaiswal, N. Patel, D.C. Kothari, A. Miotello, Appl. Catal. B: Environ. 126 (2012) 47–54.
[45] M. Gurulakshmi, M. Selvaraj, A. Selvamani, P. Vijayan, N.R.S. Rekha, K. Shanthi, Appl. Cata. A: Gen. 449 (2012) 31–46.
[46] M.K. Jeon, J.W. Park, M. Kang, J. Ind. Eng. Chem. 13 (2007) 84–91.
[47] K.P.O. Mahesh, D.H. Kuo, B.R. Huang, M. Ujihara, T. Imae, Appl. Cata. A: Gen. 475 (2014) 235–241.
[48] E.S. Aazam, Ceram. Int. 40 (2014) 6705–6711.
[49] B. Wang, G. Zhang, X. Leng, Z. Sun, S. Zheng, J. Hazard. Mater. 284 (2015) 212–220.
[50] R. Jaiswal, J. Bharambe, R. Patel, A. Dashora, D.C. Kothari, A. Miotello, Appl. Catal. B: Environ. 168–169 (2015) 333–341.
[51] Y. Zou, S.Z. Kang, X. Li, J. Qin, M. Mu, Int. J. Hydrogen Energy 39 (2014) 15403–15410.
[52] W.T. Chen, V. Jovic, D. Sun-Waterhouse, H. Idriss, G.I.N. Waterhouse, Int. J. Hydrogen Energy 38 (2013) 15036–15048.
[53] L. Laokiat, P. Khemthong, N. Grisdanurak, P. Sreearunothai, W. Pattanasiriwisawa, W. Klysubun, Korean J. Chem. Eng. 29 (2012) 377–383.
[54] J. Tauc, R. Grigorovici, A. Vancu, Phys. Status Solidi 15 (1996) 627–637.
[55] C. Karunakaran, G. Abiramasundari, P. Gomathisankar, G. Manikandan, V. Anandi, J. Colloid Interface Sci. 352 (2010) 68–74.
[56] A. Yousef, N.A.M. Barakat, T. Amna, S.S. Al-Deyab, M.S. Hassan, A. Abdel-Hay, H.Y. Kim, Ceram. Int. 38 (2012) 4525–4532.
[57] D. Barreca, P. Fornasiero, A. Gasparotto, V. Gombac, C. Maccato, T. Montini, E. Tondello, ChemSusChem 2 (2009) 230–233.
[58] M. Takeuchi, M. Hidaka, M. Anpo, J. Hazard. Mater. 237–238 (2012) 133–139.
[59] b.Y Lee, S.H. Park, S.C. Lee, M. Kang, S.J. Choung, Catal. Today 93–95 (2004) 769–776.
[60] J.V. Durme, J. Dewulf, K. Demeestere, C. Leys, H.V. Langenhove, Appl. Catal. B: Environ. 87 (2009) 78–83.
[61] L. Zhang, W.A. Anderson, S. Sawell, C. Moralejo, Chemosphere 68 (2007) 546–553.
[62] Y. Ku, K.Y. Tseng, W.Y. Wang, Water Air Soil Pollut. 168 (2005) 313–323.